J. Fluid Mech. (2007), *vol.* 591, *pp.* 461–479.
doi:10.1017/S0022112007008336 Printed in the United Kingdom

Experimental investigation into the routes to bypass transition and the shear-sheltering phenomenon

DOMHNAILL HERNON[1]†, EDMOND J. WALSH[1] AND DONALD M. MCELIGOT[2,3]

[1]Stokes Research Institute, Department Mechanical and Aeronautical Engineering, University of Limerick, Ireland

[2]Idaho National Laboratory (INL), Idaho Falls, Idaho 83415-3885 and University of Arizona, AZ 85721, USA

[3]University of Stuttgart, D-70550, Stuttgart, Germany

(Received 20 July 2006 and in revised form 17 July 2007)

The objective of this investigation is to give experimental support to recent direct numerical simulation (DNS) results which demonstrated that in bypass transition the flow first breaks down to turbulence on the low-speed streaks (or so-called negative jets) that are lifted up towards the boundary-layer edge region. In order to do this, wall-normal profiles of the streamwise fluctuation velocity are presented in terms of maximum positive and negative values over a range of turbulence intensities (1.3–6 %) and Reynolds numbers for zero pressure gradient flow upstream of, and including, transition onset. For all turbulence intensities considered, it was found that the peak negative fluctuation velocity increased in magnitude above the peak positive fluctuations and their positions relative to the wall shifted as transition onset approached; the peak negative value moved towards the boundary-layer edge and the peak positive value moved toward the wall. An experimental measure of the penetration depth (PD) of free-stream disturbances into the boundary layer has been gained through the use of the skewness function. The penetration depth (measured from the boundary-layer edge) scales as $PD \propto (\omega Re_x \tau_w)^{-0.3}$, where ω is the frequency of the largest eddies in the free stream, Re_x is the Reynolds number of the flow based on the streamwise distance from the leading edge and τ_w is the wall shear stress. The parameter dependence demonstrated by this scaling compares favourably with recent solutions to the Orr–Sommerfeld equation on the penetration depth of disturbances into the boundary layer. The findings illustrate the importance of negative fluctuation velocities in the transition process, giving experimental support to suggestions from recent DNS predictions that the breakdown to turbulence is initiated on the low-speed regions of the flow in the upper portion of the boundary layer. The representation of pre-transitional disturbances in time-averaged form is shown to be inadequate in elucidating which disturbances grow to cause the breakdown to turbulence.

† Present address: Bell Laboratories Ireland (BLI), Alcatel-Lucent, Blanchardstown Industrial Park, Dublin 15, Ireland. hernon@Alcatel-Lucent.com.

1. Introduction

1.1. *Background*

The modes of bypass transition have been elucidated through recent analytical solutions to the Orr–Sommerfeld equation and through extensive direct numerical simulation (DNS) studies which have shown that the flow first breaks down into turbulent motion on the low-speed regions of the flow near the boundary-layer edge (Jacobs & Durbin 2001; Brandt, Schlatter & Henningson 2004; Zaki & Durbin 2005); however, a caveat to this work is the lack of experimental evidence to corroborate such results. Owing to the stochastic generation of disturbances in the free stream and boundary layer, gaining experimental insight into such complex fluid behaviour in real-life test conditions is difficult. The current experimental investigation aims to provide some further insight into the breakdown from laminar to turbulent flow under grid-generated turbulence conditions.

1.2. *Experimental studies*

To date, experimental work into the bypass transition process has demonstrated that under the influence of elevated free-stream turbulence (FST) the laminar boundary layer develops high- and low-speed fluctuations relative to the mean streamwise velocity that are extended in the streamwise direction and are termed streaky structures. These streaky structures were first described by Klebanoff (1971) and their time-averaged representations are termed Klebanoff modes (due to Kendall 1985). Under certain conditions, the streaky structures have been shown to develop a streamwise waviness which eventually breaks down into a turbulent spot, as shown in the flow visualizations of Matsubara & Alfredsson (2001) and the direct numerical simulations (DNS) of Brandt *et al.* (2004). The effects of elevated FST on the underlying boundary layer have been studied for some time, Dryden (1937) is an early example. The importance of elevated free-stream turbulence intensity at the plate leading edge (Tu), usually greater than 1 %, in the bypass-transition process has been further demonstrated by Fransson, Matsubara & Alfredsson (2004) who showed that the initial disturbance energy in the boundary layer is proportional to Tu^2 and the transition Reynolds number is inversely proportional to Tu^2.

A number of experimental studies have demonstrated the evolution of structures with associated negative fluctuation velocity from the near-wall region towards the boundary-layer edge (Wygnanski, Sokolov & Friedman 1976; Blair 1992; Kendall 1998; Westin *et al.* 1998; Chong & Zhong 2005). Well upstream of transition onset, Blair (1992) observed large-scale structures with associated negative fluctuation velocities near the boundary-layer edge region; Blair termed these structures negative spikes. Approaching the point of transition onset, the negative spikes developed high-frequency components and Blair commented that the demarcation between multiple negative spikes and a turbulent structure became 'blurred'. Chong & Zhong (2005) investigated artificially generated turbulent spots and showed that high-frequency negative fluctuations develop near the boundary-layer edge before any near-wall positive fluctuations are observed; however, the question still remains as to the connection between artificially and naturally occurring turbulent spots.

1.3. *Numerical studies*

DNS studies have been a major influence in elucidating the routes to bypass transition (see e.g. Wu *et al.* 1999; Jacobs & Durbin 2001; Brandt *et al.* 2004; Zaki & Durbin 2005). These studies have illustrated that the low-speed components of the flow lift away from the wall towards the boundary-layer edge owing to the upward motion of

the vortical structures found in the free-stream region. In DNS terminology, the low-speed streak regions are termed negative or backward jets because their associated instantaneous velocity (U) is significantly less than the local mean value ($\overline{U}$), therefore such structures have negative fluctuation velocity (u). When the low-speed streaks reach the outer region of the boundary layer, they are subject to inflection-point instability and a form of Kelvin–Helmholtz type instability develops (Zaki & Durbin 2005). At this stage, the flow is locally unstable to the high-frequency disturbances contained in the free stream and eventually breaks down into a turbulent spot at the boundary-layer edge region. This route to bypass transition differs significantly from those presented before the application of DNS, where it was believed that turbulent structures were generated owing to local flow separation in the near-wall region (Roach & Brierley 2000; Johnson 2001).

The importance of the frequency content of the free-stream flow has also been demonstrated using DNS. Zaki & Durbin (2005) showed that one strongly coupled low-frequency mode and one weakly coupled high-frequency mode in the free stream were required in order to completely simulate the transition process. Brandt *et al.* (2004) demonstrated that, by varying the energy spectrum of the free-stream disturbances, the transition location moved to lower Reynolds numbers when the integral length scale of the FST was increased, comparable to the experimental results of Jonas, Mazur & Uruba (2000). To date however, experimental evidence supporting such findings is lacking and equally difficult to obtain.

1.4. *Theoretical studies and the receptivity process*

Landahl (1975, 1980) was the first to propose a physical explanation for the streak-growth mechanism through the linear lift-up effect. Theoretical studies of algebraic or transient growth (Andersson, Breggren & Henningson 1999; Luchini 2000) have since predicted that the energy growth of the optimal perturbations is proportional to the distance from the leading edge. These theories on optimal perturbations also accurately predict the wall-normal shape of the streamwise fluctuations and show that streamwise vortices in the free stream are the cause of maximum growth of the high- and low-speed streaky structures in the boundary layer. Again, the importance of the free-stream turbulence structure is noted.

The manner by which external disturbances affect the underlying laminar boundary layer is termed receptivity (Klebanoff 1971; Kendall 1998; Westin *et al.* 1998; Saric, Reed & Kerschen 2002). More recently, the study of receptivity has gained a renewed vigour mainly because of the developments in the theory of shear sheltering (Jacobs & Durbin 1998; Hunt & Durbin 1999; Maslowe & Spiteri 2001; Zaki & Durbin 2005). Jacobs & Durbin (1998) solved the model problem of a two-dimensional Orr–Sommerfeld disturbance about a piecewise linear velocity profile and determined that the penetration depth (PD) of disturbances (defined as the point where the disturbance eigenfunction (ϕ) dropped and remained below 0.01) from the free stream into the boundary layer is given by $PD \propto (1/\omega R)^{-0.133}$, where ω and R are the frequency of the largest free-stream disturbances and the Reynolds number of the flow. This dependence was also demonstrated in Maslowe & Spiteri (2001) for varying pressure gradients. Zaki & Durbin (2005) further enhanced the concept of PD by introducing a coupling coefficient which represented better the interaction between the free-stream disturbances and the underlying boundary layer. To further complicate any investigation into the receptivity process, there are a number of parameters that affect it. Some of the more critical parameters are the FST intensity and turbulent length scales, the degree of isotropy of the FST and the leading-edge geometry plays a

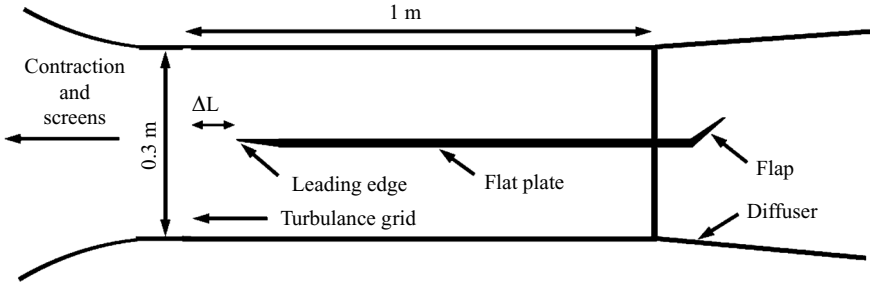

FIGURE 1. Illustration of experimental arrangement (not to scale). ΔL is the plate leading-edge distance downstream of the grids.

critical role also (Hammerton & Kerschen 1996; Westin *et al.* 1998; Kendall 1998; Saric *et al.* 2002; Fransson 2004, discuss the importance of the leading edge in the receptivity process).

The current investigation analyses, in a unique way, pre-transitional wall-normal profiles of the streamwise fluctuating velocity over a range of turbulence intensities and Reynolds numbers. This investigation gives experimental support to recent DNS results which demonstrated that lifted low-speed streaks are the initiation sites of turbulent spot production. This is achieved by examining the variation in disturbance magnitude between the low- and high-speed streaks as transition onset is approached. We also illustrate how crucial information is lost through the time-averaging process commonly presented in the literature, i.e. the Klebanoff mode disturbance profiles. Finally, the skewness parameter is implemented throughout the boundary-layer thickness to give an experimental measure of the change in receptivity of a laminar boundary layer when under the influence of elevated FST.

2. Experimental facility and measurement techniques

2.1. *Experimental facility*

The test surface for the current measurements is a flat plate manufactured from 10 mm thick aluminium approximately 1 m long by 0.295 m wide and is placed in the centre of the test section. The leading edge is semi-cylindrical and 1 mm in radius. Figure 1 provides the experimental arrangement. The flow over the flat plate was qualified as two-dimensional over all measurement planes. The design of the trailing-edge flap was shown to anchor the stagnation streamline on the upper test surface, thus allowing for zero-pressure gradient to be established, facilitating excellent comparison against Blasius theory. The effectiveness of the leading-edge design was confirmed by considering that the bulk pressure distribution along the length of the plate varies no more than 1 %, except for the most upstream static pressure point, located 30 mm downstream of the leading edge, where a 5 % drop in dynamic pressure was measured. Further details on the design, manufacture and characterization of the turbulence grids and the flat plate (including flow visualization using both oil-powder and shear-sensitive liquids crystals) can be found in Walsh *et al.* (2005).

All measurements were obtained in a non-return wind tunnel with continuous airflow supplied by a centrifugal fan. Maximum velocities in excess of $100\,\mathrm{m\,s^{-1}}$ can be achieved. The settling chamber consists of honeycomb and wire-gauze grids which enable the reduction of flow disturbances generated by the fan. Using hot-wire anemometry, low-pass filtered at 3.8 kHz, the background turbulence intensity in the

Parameter	PP Grid 1	PP Grid 2	SMR
Grid bar width (d) (mm)	7	2.6	0.5
Mesh length (M) (mm)	34	25.2	2.5
%Grid solidity	37	20	36
$\%Tu_{min}$	4	2	0.4
$\%Tu_{max}$	7	4.3	3
$\Lambda_{x(min)}$ (mm)	9	5	5
$\Lambda_{x(max)}$ (mm)	19	15	7.5

TABLE 1. Geometric description of turbulence grids and range of turbulence characteristics available, where Λ_x is the streamwise integral length scale. PP and SMR relate to the structure of the turbulence grids where PP refers to perforated plate and SMR refers to square mesh array of round wires.

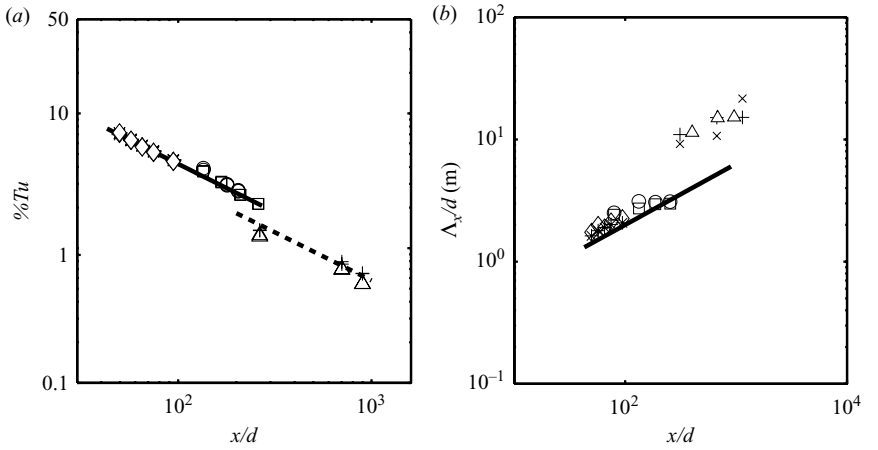

FIGURE 2. (*a*) Turbulence decay for all three grids, PP1, PP2 and SMR compared to the Roach (1987) correlations. (*b*) Integral length-scale evolution compared to the Roach (1987) correlations. ◇, PP1, $Re_d = 6000$; *, PP1, $Re_d = 2600$; ○, PP2, $Re_d = 760$; □, PP2, $Re_d = 1310$; +, SMR, $Re_d = 119$; △, SMR, $Re_d = 265$; ——, $\%Tu = 1.13(x/d)^{-5/7}$; - - -, $\%Tu = 0.8(x/d)^{-5/7}$. In (*b*) ——, $\Lambda_x/d = 0.2(x/d)^{0.5}$. ×, Estimation of Λ_x using (2.3) for the SMR grid. Re_d is the Reynolds number based on the diameter of the hot-wire probe.

working section of the tunnel was measured to be 0.2 %. The test section dimensions are 1 m in length by 0.3 m width and height.

Table 1 gives the turbulence grid dimensions and the associated range in FST intensities and scales. The turbulence grids are placed at the test-section inlet. All grids were designed and qualified according to the criteria of Roach (1987). The plate's leading edge was always placed at least 10 mesh lengths downstream of the grid (ΔL in figure 1) and the isotropy of the free-stream turbulence was validated by comparison to the von Kármán one-dimensional isotropic approximation given by Hinze (1975), with good agreement. The turbulence decay downstream of the turbulence grids compares favourably to the power-law relation of Roach (1987) where the percentage turbulence intensity decays to the power of $-5/7$ (figure 2*a*). The streamwise integral length scale (Λ_x) is calculated by

$$\Lambda_x = U_\infty \int_0^\infty R(T)\,\mathrm{d}T, \tag{2.1}$$

where $R(T)$ is the autocorrelation function which is given by

$$R(T) = \frac{\overline{u(t)u(t-T)}}{\overline{u}^2}, \tag{2.2}$$

and this equation calculates the correlation between the streamwise velocity fluctuations at a fixed point in the flow at two different times, t and $t - T$. The overbar represents the time-average value. The areas under the autocorrelation curves were calculated until the first time $R(T)$ reached zero to give a measure of the integral length scales according to (2.1). The downstream distribution of Λ_x is shown in figure 2(*b*) and, once again, good agreement between the measurements and the correlation of Roach (1987) is observed for the PP grids. As illustrated in figure 2(*b*), the estimation of Λ_x using (2.1) compared to within 20 % of the isotropic estimation by Hinze (1975) given by

$$\Lambda_x = \left[\frac{E(f)U_\infty}{4\overline{u}^2}\right]_{f\to 0}, \tag{2.3}$$

thereby further illustrating the degree of isotropy of the FST.

2.2. *Measurement techniques*

Mean and fluctuating streamwise velocities were measured using a constant temperature anemometer (A.A. Lab Systems AN-1005). Hot-wire and hot-film probes were operated at overheat temperatures of 250 °C and 110 °C, respectively. All boundary-layer measurements were recorded over 10 s periods at a sampling frequency of 10 kHz and were low-pass filtered at 3.8 kHz to eliminate any noise components at higher frequencies. During any boundary-layer traverse, the temperature in the test section was maintained constant to within 0.1 °C. Variation in fluid temperature was compensated by using the technique of Kavence & Oka (1973). The hot-wire calibration was obtained using King's law between test velocities of 0.4 m s^{-1} and 20 m s^{-1}.

In the current investigation, transition onset was defined to occur with the observation of approximately one turbulent spot in every 10 s. Using the method of Ubaldi *et al.* (1996) the onset of transition was detected using a hot-film sensor placed at the wall (Dantec 55R47) whereby a turbulent spot was determined by increased heat transfer from the sensor. The dual-slope method of Kuan & Wang (1990) was implemented and the near-wall intermittency (γ) was determined to be approximately 0.1 % (see e.g. Hernon, Walsh & McEligot 2006). Using this technique, it was found that the Reynolds number at which transition begins compared favourably to both the well-established correlation of Mayle (1991) and the recent correlation of Fransson *et al.* (2005), figure 3. The variation in the transition onset Reynolds numbers at constant $\%Tu$ may be explained as being due to the variation in free-stream to boundary-layer scales with varying free-stream velocity. The boundary layer become thinner with increased velocity whereas the integral length scale remains constant. This is similar to Brandt *et al.* (2004) where it was demonstrated that varying the free-stream integral length scales changed the transition onset Reynolds number considerably.

3. Results and discussion

3.1. *Pre-transitional flow characteristics*

Figure 4(*a*) illustrates the variation in frequency content and disturbance amplitude of the flow from the near-wall to the boundary-layer edge and free-stream regions.

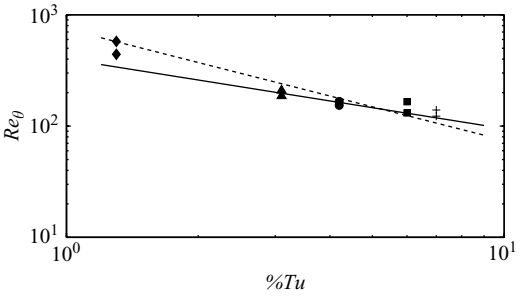

FIGURE 3. Comparison of transition onset Reynolds numbers against the transition onset correlations of Mayle (1991) and Fransson *et al.* (2005). ◆, $Re_\theta = 442 - 577$, $Tu = 1.3\,\%$; ▲, $Re_\theta = 186 - 209$, $Tu = 3.1\,\%$; ○, $Re_\theta = 154 - 167$, $Tu = 4.2\,\%$; ■, $Re_\theta = 131 - 166$, $Tu = 6\,\%$; +, $Re_\theta = 123 - 139$, $Tu = 7\,\%$. ——, Mayle (1991) correlation, $Re_\theta = 400Tu^{-5/8}$. - - -, Fransson *et al.* (2005) correlation, $Re_\theta = 745/Tu$, at $\gamma = 0.1$.

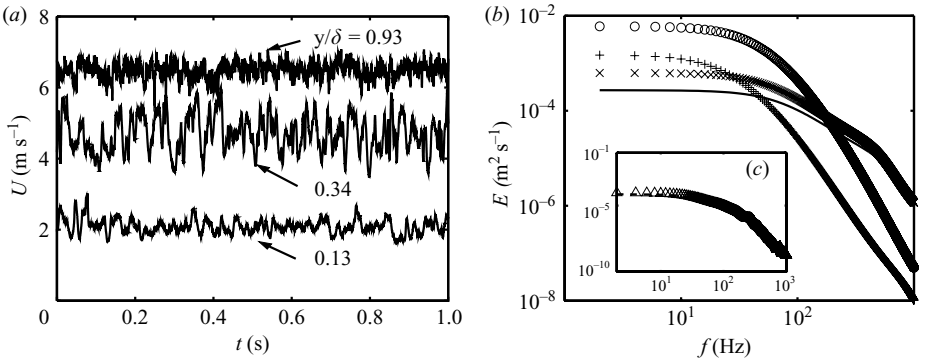

FIGURE 4. (*a*) Velocity traces from the near-wall to the free-stream region at $Tu = 3.1\,\%$ and $Re_\theta = 186$ (near transition onset). (*b*) Energy spectra for the same conditions as figure 4(*a*). +, $y/\delta = 0.13$; ○, $y/\delta = 0.34$; ×, $y/\delta = 0.93$; ——, $y/\delta = 1.2$. (*c*) $Re_\theta = 106$. △, $y/\delta = 1$; - - -, $y/\delta = 1.2$.

The effects of shear sheltering are apparent as the high-frequency content of the flow is filtered by the boundary-layer shear as the wall is approached. In the near-wall region, the flow structures are low in frequency; similar results were found by Matsubara & Alfredsson (2001) and Jacobs & Durbin (2001). Jacobs & Durbin (2001) demonstrated that the spectra of disturbances between the free stream and the wall changed markedly; in the free stream, the spectrum was pre-set owing to the superposition of modes of the Orr–Sommerfeld continuous spectrum whereas in the boundary layer, the spectrum shifted to even lower frequencies than those present in the free stream. The most notable features of the velocity traces are the large reductions in the instantaneous velocity at $y/\delta \approx 0.93$. The cause of the reduction in instantaneous velocity could be due to free-stream vortices that penetrate the upper region of the boundary layer or low-speed streaks being lifted up to the boundary-layer edge region. These negative structures are qualitatively similar to the negative spikes reported in Blair (1992) and have a scale of approximately 10δ, where δ is defined as the boundary-layer thickness. As in the experiment by Blair, at upstream locations, single and double negative spikes were observed in the current investigation. The shear sheltering phenomenon is most evident in figure 4(*b*) where,

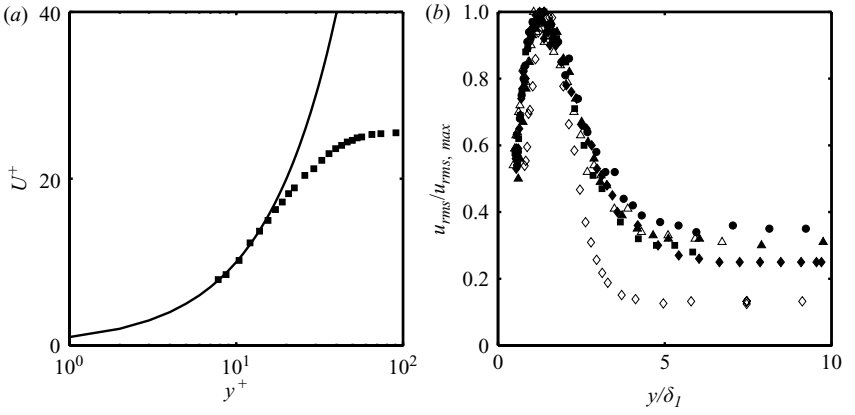

FIGURE 5. (*a*) Velocity profile at $Tu = 3.1\,\%$ compared to linear law of the wall. ——, linear law of the wall; ■, measured velocity profile. (*b*) Normalized r.m.s. disturbance profiles indicative of the Klebanoff mode. ◇, $Tu = 1.3\,\%$, $Re_\theta = 577$; ▲, $Tu = 3.1\,\%$, $Re_\theta = 209$; ◆, $Tu = 4.2\,\%$, $Re_\theta = 167$; ○, $Tu = 6\,\%$, $Re_\theta = 166$; △, $Tu = 7\,\%$, $Re_\theta = 139$.

at the higher frequencies, the spectra at $y/\delta \approx 1$ (near the boundary-layer edge region) and at $y/\delta \approx 1.2$ (in the free-stream region) are almost identical; however, at the lower frequencies, the flow near the boundary-layer edge region has higher energy content than the free stream. The free-stream flow does not contain these large-scale structures, which indicates that such structures must originate from within the boundary layer. Figure 4(*c*) demonstrates that well upstream of transition onset, the spectra at the boundary-layer edge and in the free stream are almost identical over the whole range of frequencies, thus demonstrating the change in flow structure as the point of breakdown nears. Results consistent with figure 4 were observed over the whole range of turbulence intensities considered in this investigation.

Figure 5(*a*) demonstrates a sample velocity profile in wall units compared to the linear law of the wall. It is clear that the near-wall measurement resolution is of sufficient accuracy to provide for accurate determination of the wall shear stress (τ_w). Figure 5(*b*) illustrates the r.m.s. disturbance profiles at transition onset over the range of turbulence intensities considered. The profiles are indicative of the Klebanoff mode which is a time-average representation of the streaky structures in the flow. The profiles agree well with the experimental results of Matsubara & Alfredsson (2001), the DNS of Brandt *et al.* (2004) and the theoretical representations by Andersson *et al.* (1999) and Luchini (2000), where the amplitude maximum is observed at $y/\delta_1 \approx 1.4$ (δ_1 is the boundary-layer displacement thickness) and the peak r.m.s. velocity fluctuations are approximately 10 % of the free-stream velocity (U_∞).

3.2. *Instantaneous velocity fluctuation profiles*

In the previous section, the r.m.s. streamwise velocity fluctuation profiles (Klebanoff mode) were presented; however, the result of such data processing is to mask the effects of both positive and negative fluctuations. Wundrow & Goldstein (2001) commented on the significance of looking at maximum disturbance magnitudes compared to r.m.s. values when considering what disturbances are critical in causing the transition to turbulence. Similar to Brandt *et al.* (2004), we will define a quantity that illustrates better the magnitude of the most prominent disturbances found in pre-transitional flow. The maximum positive and negative values of the local

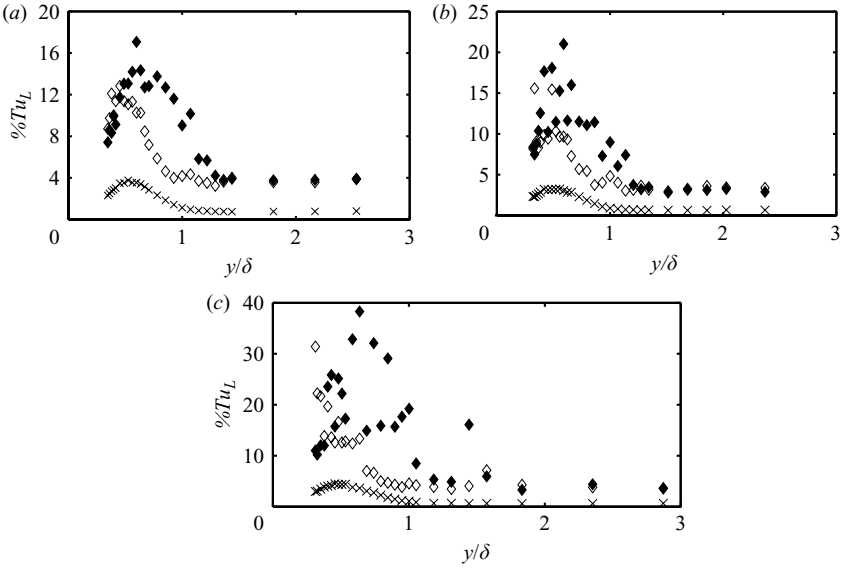

FIGURE 6. Maximum positive and negative fluctuation velocities presented in terms of a local disturbance intensity (%Tu_L) at $Tu = 1.3\,\%$. (*a*) $Re_\theta = 352$. (*b*) $Re_\theta = 392$. (*c*) $Re_\theta = 577$ (transition onset). ◆, maximum negative value; ◇, maximum positive value; ×, r.m.s. value.

streamwise fluctuating velocity are presented in figure 6 for three streamwise positions at $Tu = 1.3\,\%$. Figure 6(*a*) demonstrates that well upstream of transition onset, the magnitude of the maximum positive fluctuation velocity is below the maximum negative fluctuation velocity, where the peak positive value is $Tu_L \approx 13\,\%$ at $y/\delta \approx 0.45$ and the peak negative value is $\%Tu_L \approx 18$ at $y/\delta \approx 0.6$. $\%Tu_L$ is referred to as a local disturbance magnitude and is given by $\%Tu_L = max|u_{positive/negative}|/U_\infty \times 100$. It can be seen that the disturbance magnitudes of the low- and high-speed streaks (defined as regions with U below and above $\overline{U}$, respectively) are far above that indicated by the r.m.s. values. As the point of transition onset is approached, the magnitudes of the maximum positive and negative disturbances far exceed those indicated by the r.m.s. values, where the peak r.m.s. disturbance is approximately 4 % of U_∞ (figure 6*b*). Also evident is the increase in magnitude of the negative value above the positive and a slight shift in the peak locations. These attributes are even more pronounced at transition onset (figure 6*c*), where the peak disturbance magnitude associated with the negative fluctuation velocity is $Tu_L \approx 40\,\%$, and the peak disturbance magnitude associated with the positive fluctuation velocity is approximately $Tu_L \approx 30\,\%$. The shift in the relative peak positions is also evident in figure 6(*c*) where the peak negative value is located at $y/\delta \approx 0.6$ and the peak positive value is located at $y/\delta \approx 0.3$. In figure 6(*c*), the flow is at transition onset and therefore some of the traces contain turbulent structures, hence the scatter in the results. However, note how the trends associated with the low- and high-speed streaks are similar to the upstream measurements, even when turbulent structures are present.

Similar to figure 6, figure 7 presents the disturbance magnitudes of the maximum positive and negative fluctuating velocities at $Tu = 6\,\%$. It is evident that, even at much higher turbulence intensities, the same trends are observed; as transition onset is approached, the magnitude of the negative value exceeds the positive value and the peak negative value moves towards the boundary-layer edge ($y/\delta \approx 0.6$) and the peak

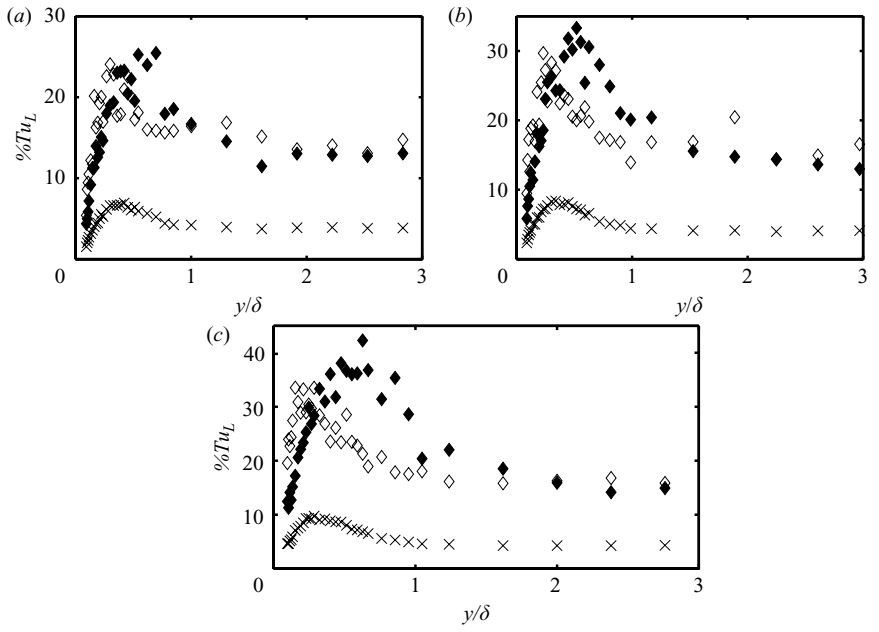

FIGURE 7. Maximum positive and negative fluctuation velocities presented in terms of a local disturbance intensity ($\%Tu_L$) at $Tu = 6\,\%$. (*a*) $Re_\theta = 83$. (*b*) $Re_\theta = 107$. (*c*) $Re_\theta = 131$ (transition onset). ◆, maximum negative value; ◇, maximum positive value; ×, r.m.s. value.

Time range (s)	0–2	2–4	4–6	6–8	8–10
$\%Tu_L$	12	17.1	13.7	13	11.5
Average $\%Tu_L$	13.5				

TABLE 2. Comparison between the peak maximum positive disturbances over each 2 s trace and average of the five 2 s traces.

positive value moves towards the wall ($y/\delta \approx 0.3$). Similar results for the $Tu = 3.1\,\%$ and $Tu = 7\,\%$ test cases were also observed.

The results presented in figure 6(*c*) have a large degree of scatter compared to those of figure 7. This increased scatter occurs because at this lower turbulence intensity a higher free-stream velocity is required in order to cause the flow to transition on the surface of the plate. At this higher free-stream velocity/low turbulence intensity, the amplitudes of the turbulent spots are far greater than the mean amplitude of the surrounding laminar flow. Therefore, when the flow breaks down into turbulent patches, the highly stochastic nature of the flow is illustrated further at the lower turbulence intensities when examining instantaneous measurements such as those given in figure 6(*c*). Because of the random nature of the disturbance generation, the sample time will significantly effect the peak disturbance magnitudes. In order to estimate the uncertainty in the measurements owing to the variation in the sample size, each 2 s portion of the 10 s trace was analysed separately and the variation in the peak disturbance magnitude was recorded. This was carried out for the $Tu = 1.3\,\%$ test case at $Re_\theta = 352$ (figure 6*a*) and the values obtained are given in table 2. Over the 10 s trace, the absolute maximum peak negative disturbance was $Tu_L = 17.1\,\%$. The

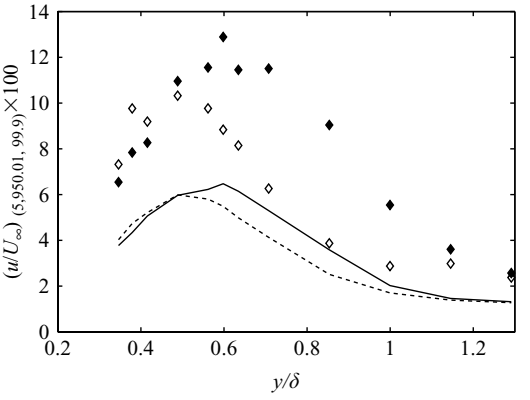

FIGURE 8. Statistical distribution of the 5th, 95th, 0.1st and 99.9th levels for $Tu = 1.3\,\%$ and $Re_\theta = 352$. ◆, 0.1st; ◇, 99.9th; ——, 5th; - - -, 95th.

peak disturbance when all five 2 s measurements were averaged was $Tu_L = 13.5\,\%$ and the absolute minimum value recorded by any 2 s trace was $Tu_L = 11.5\,\%$. The important point here is that the sample time should be long enough to capture at least one of the peak disturbances. In the current investigation that sample time was 10 s.

Another method of investigating the magnitudes of the disturbances and also of reducing the uncertainty in data could be to examine the distribution of the 5th and 95th statistical distributions (figure 8). On examining these distributions, it was found that the 5th and 95th levels were up to 65 % less than the maximum positive and negative instantaneous disturbances compared to figure 6(*a*). It is also shown that taking even higher-order statistics does not sufficiently account for the peak disturbances where the 0.1st and 99.9th levels were 25 % less that those of figure 6(*a*). This suggests that such distributions do not give a proper sense of what disturbances are most likely to initiate the breakdown to turbulence.

A number of important observations have been made concerning the transition process so far. Taking mean statistics is not sufficient in fully explaining the routes to bypass transition. Furthermore, low- and high-speed streaks are clearly different physical mechanisms, hence by examining the r.m.s. of the flow, the understanding of the physical processes initiating turbulent spot production is lost. In this investigation, the peak disturbance associated with the negative fluctuation velocity was $Tu_L \approx 40\,\%$ and the peak disturbance associated with the positive fluctuation velocity was $Tu_L \approx 30\,\%$ at transition onset for all turbulence intensities considered. Moreover, the relative positions of the peak positive and negative fluctuation velocities associated with the low- and high-speed streaks also vary considerably as transition onset is approached. The peak negative value moved toward the boundary-layer edge and the peak positive value moved toward the wall, this phenomenon has also been observed by Brandt *et al.* (2004). It was demonstrated in the current investigation that the low-speed streak amplitudes near the boundary-layer edge are much greater than 26 % of the free-stream velocity; according to Andersson *et al.* (1999) and Brandt *et al.* (2004) this value is high enough for secondary instabilities to develop on the streaks, thus causing the onset of transition. Since transition onset is based upon the stability of an event in the boundary layer, it appears a reasonable argument that the location of transition onset will be in the region of greatest instability. The measurements of figures 6 and 7 suggest that the greatest instabilities are associated with the negative structures in the outer region of the boundary layer where the shear

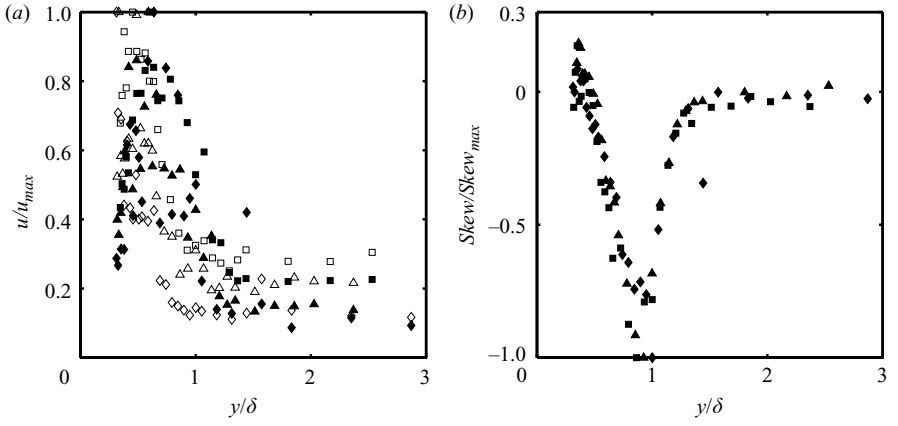

FIGURE 9. (*a*) Wall-normal disturbance profiles of the low- and high-speed streaks. (*b*) Skewness distribution for the same conditions as in (*a*). △, $Re_\theta = 352$; □, $Re_\theta = 392$; ◇, $Re_\theta = 577$. In (*a*) open symbols are maximum positive values and filled symbols are maximum negative values. All measurements are at $Tu = 1.3\,\%$.

stress is at its minimum and hence this is the region where turbulent spots form. Again, such an argument cannot be deduced by examining the r.m.s. signal alone. In the near-wall region, the damping due to the wall shear is pronounced and therefore the breakdown to turbulence is less likely to occur in this region.

Another interesting point illustrated in figures 6 and 7 is that the laminar boundary layer will observe significant variation in the peak turbulence intensity levels in the free stream of approximately 20 %. This random high-intensity forcing from the free stream will drastically alter the response of the underlying laminar boundary layer.

3.3. *Normalized fluctuation velocity and skewness profiles*

Considerable theoretical effort has been invested in understanding how disturbances from the free stream act on and penetrate the laminar boundary layer to cause transition (see e.g. Andersson *et al.* 1999; Hunt & Durbin 1999; Luchini 2000; Jacobs & Durbin 2001; Brandt *et al.* 2004; Zaki & Durbin 2005). Extensive information has been gained through these studies; however, experimental evidence to support such postulations has not been forthcoming because of the inherent difficulties in obtaining detailed measurements to validate theoretical or DNS studies. It is the objective of this section to provide an experimental measure of the penetration depth (PD) of the largest disturbances into the boundary layer and compare this to recent theoretical developments, thereby leading to increased knowledge of the flow evolution to transition.

Figure 9(*a*) illustrates normalized profiles of the maximum positive and negative velocity fluctuations associated with the low- and high-speed streaks as the boundary layer proceeds towards transition onset (previously presented in figure 6) where each positive and negative fluctuation velocity is normalized with the peak value at that streamwise position (u_{max}). Therefore, as figure 5(*b*) represents the shape of the Klebanoff mode, figure 9(*a*) represents the signatures of the high- and low-speed streaks. In figure 9(*a*), the scatter in the distributions is considerable, for reasons discussed previously, and therefore the trends in the results are not so clear. The maximum negative values collapse somewhat and all peak at $y/\delta \approx 0.6$, whereas the peak positive values display much more scatter with a peak range of $y/\delta \approx 0.3$–0.5. Figure 9(*b*) represents the skewness of the results normalized with respect to

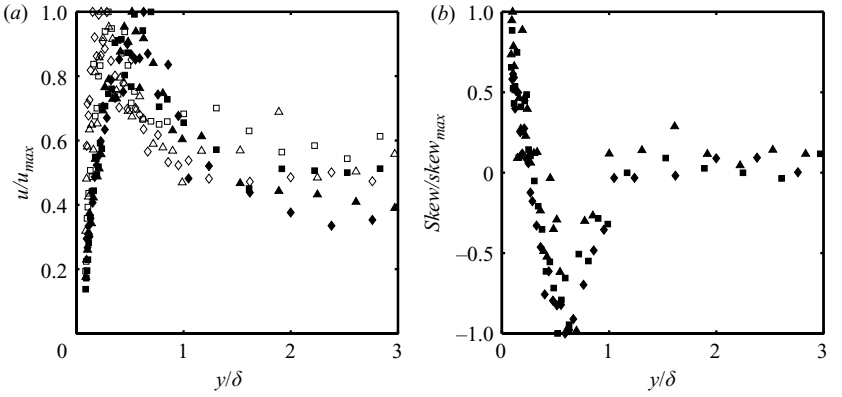

FIGURE 10. As for figure 9, but △, $Re_\theta = 83$; □, $Re_\theta = 107$; ◇, $Re_\theta = 131$ and measurements are at $Tu = 6\,\%$.

the maximum skewness at each streamwise position. The skewness is defined as $Skew = (U - \bar{U})^3/u_{rms}^3$, where U is the instantaneous velocity, $\bar{U}$ is the mean velocity and u_{rms} is the r.m.s. fluctuation velocity. The skewness represents the lack of statistical symmetry in a signal or equivalently the asymmetry in the probability distribution of the observations. It is clear from figure 9(*b*) that all three profiles collapse and the maximum skewness is a negative value at each streamwise location. Therefore, figure 9(*b*) demonstrates that the negative fluctuation velocities are most prominent in the skewness profiles throughout the boundary layer, and peak at $y/\delta \approx 0.9$.

The trends in the normalized high- and low-speed streaks are more obvious in figure 10(*a*) at much higher turbulence intensity. It is apparent that, when normalized in this manner, the high-speed streak signatures collapse with a peak positive value located at $y/\delta \approx 0.25$ and the low-speed streaks collapse with a peak negative value at $y/\delta \approx 0.6$. Figure 10(*b*) demonstrates the skewness of the fluctuation velocities at the same streamwise locations. The three profiles shown in figure 10(*b*) show similar trends up to the point of maximum skewness (located at $y/\delta \approx 0.6$) and collapse reasonably well up to this point also. It must be stated here that the $Tu = 6\,\%$ case was the worst of those considered.

In figure 10(*b*), at the most upstream measurement at $Re_\theta = 83$, the peak positive and negative skewness values are approximately equal, with the peak positive located closer to the wall ($y/\delta \approx 0.1$) and the peak negative skewness located at $y/\delta \approx 0.7$. However, the two profiles closer to transition onset have negative peak skewness values. This shift from positive to negative peak skewness as the flow nears transition onset once again demonstrates the importance of negative fluctuation velocities as the flow develops to the point of turbulent spot formation and hence the breakdown to turbulence.

Table 3 is a summary of the peak locations for all of the tests considered. Shown are the peak fluctuation velocity positions of the low- and high-speed streaks. In general, the low-speed streaks peak at $y/\delta \approx 0.6$ and the high-speed streaks peak at $y/\delta \approx 0.25$. The streamwise integral length scales (Λ_x) for the current tests are also given. It can be seen from table 3 that, as the the intensity of the FST increases, the position of the peak skewness moves closer to the wall. Figure 11 is a sketch of the flow characteristics proposed to cause the peak skewness to penetrate further into the boundary layer with increased $\%Tu$ and hence, in general, with increased Λ_x, as Λ_x and $\%Tu$ are scaled with the turbulence grid bar dimension. It is proposed that the

$\%Tu$	Λ_x (m)	y/δ (u_{ls})	y/δ (u_{hs})	y/δ $(skew_{peak})$
1.3	0.005	0.64	0.45	0.93
3.1	0.0064	0.65	0.23	0.78
4.2	0.0052	0.63	0.24	0.76
6	0.011	0.63	0.23	0.63
7	0.0098	0.62	0.29	0.61

TABLE 3. Summary of the peak locations for the high-speed streaks (hs), the low-speed streaks (ls) and the peak skewness values. The peak locations are given as an average over the range presented.

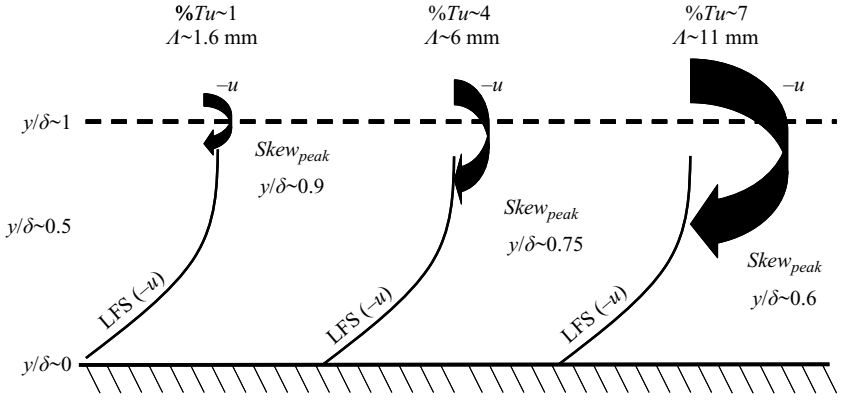

FIGURE 11. The interaction between the lifted low-speed streaks and free-stream vortices. LFS denotes the lifted low-speed streaks.

low-speed streaks (negative jets) are lifted up to the boundary-layer edge region. At low $\%Tu$, the free-stream eddies are relatively small in comparison to the boundary-layer thickness. Furthermore, near the boundary-layer edge region, the shear stress at the lowest $\%Tu$ level is large and the free-stream eddies will not penetrate far into the boundary layer because of the shear sheltering effect. At the point when the eddies interact with the lifted low-speed streaks ($y/\delta \approx 0.9$), the skewness is at its maximum and is negative because both structures have negative fluctuation velocity ($-u$). As the turbulence intensity increases, the eddy size increases (as the turbulence grid bar dimension increases) and the shear stress near the boundary-layer edge reduces considerably owing to the reduction in transition-onset Reynolds number at higher free-stream turbulence level. Therefore, the largest free-stream vortices, which have the lowest frequency components in the free stream indicated by the integral length scale, will penetrate further into the boundary-layer flow. At the highest $\%Tu$, the eddies are much larger than those at lower $\%Tu$ and therefore the point where the free-stream eddies interact with the lifted low-speed streaks is much further into the boundary layer ($y/\delta \approx 0.6$). This proposed physical characteristic of the flow also follows the results presented in figures 9 and 10, where the skewness profiles collapsed up to the point of maximum negative skewness whereafter the profiles deviated considerably, thereby illustrating the increased interaction between the free-stream eddies and the lifted low-speed streaks as the flow evolves towards transition onset. Therefore, in the light of the previous discussion, it was considered to use the location of

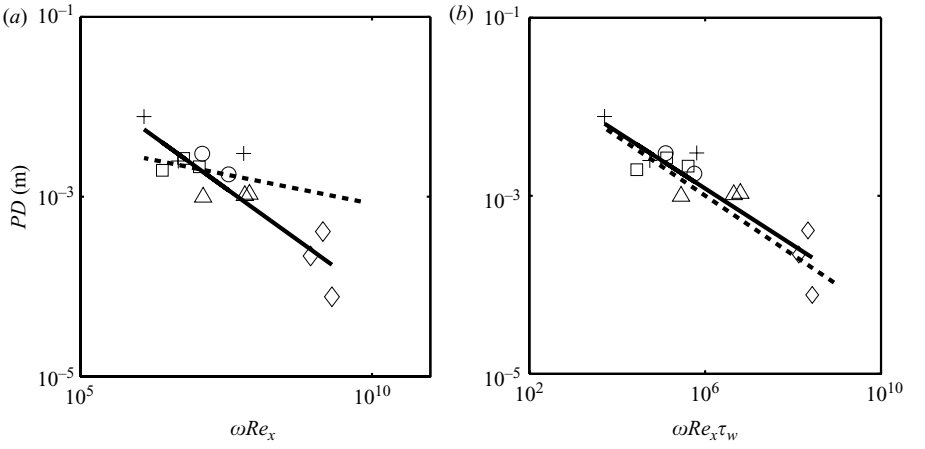

FIGURE 12. Variation of penetration depth (PD) measured from the boundary-layer edge over the range of test conditions. (*a*) ——, trend line fit to experimental data $PD \propto (\omega Re_x)^{-0.4}$. - - -, $PD \propto (\omega R)^{-0.133}$ by Jacobs & Durbin (1998). (*b*) ——, trend line fit to experimental data $PD \propto (\omega Re_x \tau_w)^{-0.3}$. - - -, $PD \propto (\omega Re_x \tau)^{-0.33}$ by Jacobs & Durbin (1998), where τ was replaced with the current experimentally measured τ_w values to allow for comparison. ◇, $Tu = 1.3\,\%$; △, $Tu = 3.1\,\%$; ○, $Tu = 4.2\,\%$; □, $Tu = 6\,\%$; +, $Tu = 7\,\%$.

peak skewness as an experimental measure of the PD of disturbances into the pre-transitional boundary layer, where the PD will be presented in physical units and measured from the boundary-layer edge.

3.3.1. *Parameter dependence for penetration depth*

Jacobs & Durbin (1998) solved the model problem of a two-dimensional Orr–Sommerfeld disturbance about a linear piecewise velocity profile and determined that the PD was the point below the boundary-layer edge where the disturbance eigenfunction (ϕ) dropped and remained below 0.01. They showed that $PD \propto (\omega Re_x \tau)^{-0.33}$, where ω is the frequency of the largest eddies in the free stream, Re_x is the Reynolds number of the flow based on the streamwise distance from the leading edge and τ is a representative shear stress based on a piecewise linear velocity profile. Substituting the approximation $\tau \backsim PD^{4.5}$ (which is obtained from Blasius flow) into the above relationship, they concluded that $PD \propto (\omega Re_x)^{-0.133}$. This model captured the dependence of the PD on frequency and Reynolds number; therefore, any experimental measure of PD should also scale accordingly, or at the very least demonstrate the same parameter dependence.

For the largest disturbances in the free stream, ω can be estimated by assuming that $\omega = c/\Lambda_x$, where c is the propagation speed of the largest disturbances in the free stream (taken to be equal to the free-stream velocity) and Λ_x is the length scale of the largest streamwise eddies in the free stream. The simplification that the disturbances in the free stream travel at the free-stream velocity is used by Jacobs & Durbin (1998) and Zaki & Durbin (2005) and is known to apply in large Re_x limits. Figure 12(*a*) illustrates the PD, which was taken as the point of maximum negative skew and measured from the boundary-layer edge, plotted against ωRe_x for all of the turbulence intensities considered in this work. It is clear that the slope of the relationship presented here does not exactly follow the results of Jacobs & Durbin (1998); however, the use of peak skewness as a measure of the penetration depth does demonstrate the expected dependence on ω and Re_x, i.e. as ω and Re_x increase,

the PD decreases. This result is at present not regarded as significant because of the difference between the current results and the analysis of Jacobs & Durbin (1998), i.e. (i) the arbitrary definition in Jacobs & Durbin (1998) of where the free-stream disturbances lose their oscillatory nature in the boundary layer; (ii) in the theory, the continuous forcing of disturbances from the free stream into the laminar boundary layer is modelled which may not be present in reality owing to the stochastic nature of grid-generated turbulence; and (iii) the most probable reason for the difference between experiment and theory is that the definition of τ and the scaling $\tau \backsim PD^{4.5}$ presented by Jacobs & Durbin (1998) were strictly functions of the Blasius velocity profile. It has been shown that the Blasius profile is not realistic in flows which are under the influence of elevated FST (see e.g. Roach & Brierley 2000; Matsubara & Alfredsson 2001; Hernon & Walsh 2007).

It was decided to incorporate a measure of the shear stress into the treatment of the current investigation, considering the shear itself is critical in determining what structures may pass through the boundary-layer edge into the boundary layer (Jacobs & Durbin 1998; Hunt & Durbin 1999). Figure 12(*b*) shows the variation of PD in terms of $\omega Re_x \tau_w$ and demonstrates that using the location of the peak skewness as a measure of the penetration depth of disturbances into the boundary layer appears to give excellent agreement with the theoretical approximation of Jacobs & Durbin (1998) given by $PD \propto (\omega Re_x \tau)^{-0.33}$; note here that the representative shear stress (τ) in the Jacobs & Durbin (1998) approximation for a piecewise linear velocity profile has been replaced with the measured τ_w values from the current investigation to allow for a non-rigorous comparison. Figure 12(*b*) demonstrates that increasing the shear, the Reynolds number or the frequency of the free-stream disturbances reduces the penetration depth of disturbances into the boundary layer. In this instance, τ_w was chosen as the representative shear stress because of its physical significance, i.e. when the Reynolds number increases, so too will the wall shear, and τ_w was obtained from the measured velocity profiles. Although in figure 12(*b*) the current PD curve is not directly comparable to the curve of Jacobs & Durbin (1998) (owing to the different definitions of the shear stress), note how well the peak skewness captures the parameter dependence for the penetration depth.

In figure 12, the correlations provided are accurate only to within $\pm 50\,\%$ and are presented only to demonstrate the trends in the results. Although this degree of correlation is acknowledged as poor, the qualitative results obtained using the location of peak skewness as a measure of the PD and its ability to demonstrate the known parameter-dependence for the change in receptivity of the boundary layer owing to elevated FST, demonstrates that using the location of peak skewness may be a way forward in characterizing the change in receptivity of a laminar boundary layer. The scatter in the results could be attributed to the stochastic nature of disturbance generation in the laminar boundary layer when under the influence of grid-generated turbulence conditions where peak instantaneous turbulence intensities in the boundary layer can reach levels as high as $Tu = 20\,\%$ (figure 7*c*). A longer sampling time may reduce the scatter level.

The previous scaling for the PD can be simplified to rely only on free-stream parameters. Schlichting (1979) gave an approximation for τ_w in terms of free-stream parameters for a Blasius boundary layer as $\tau_w = (0.332\rho U_e^2)/\sqrt{Re_x}$, thus avoiding any problems with accurate prediction of τ_w, therefore allowing for easy implementation into commercial codes. This implies that the PD can now be scaled as $(0.03\omega\rho U_e^2\sqrt{Re_x})^{-0.31}$. The inclusion of the free-stream parameters follows the correct trend in the PD and this also adds simplicity to any future computational

efforts that may wish to incorporate this modelling. This representation of the PD is based on substituting the actual τ_w measured from the velocity profiles (when under the influence of elevated FST) with the Blasius solution given by Schlichting (1979) using free-stream parameters.

4. Concluding remarks

Although DNS results have been shown to compare reasonably well to experimental results from a time-averaged perspective, e.g. plots of skin friction at low *Tu*, the DNS scenario concerning the breakdown of lifted low-speed streaks still requires experimental support. This investigation gives strong experimental support to some of the recent theoretical and numerical insights into the routes to bypass transition. It was shown that time-averaged results are not representative of the disturbance levels that may lead to the generation of turbulent spots. In order to obtain a better understanding of the physics of the disturbances that lead to transition, the current investigation examines the streamwise distributions of the maximum positive and negative fluctuation velocities over a range of free-stream turbulence intensities and Reynolds numbers across the boundary-layer thickness. Similar to the DNS results, the disturbance amplitudes representing the low- and high-speed streaks are considerably greater than those indicated by the r.m.s. values, even well upstream of transition onset. As the point of transition onset approached, it was found that the magnitudes of the peak disturbances associated with the negative fluctuation velocities increased beyond those of the positive fluctuation velocities. As the flow evolved closer to transition onset, for all turbulence intensities considered, the peak negative value was approximately 40 % of the free-stream velocity, and was greater in magnitude than the peak positive value. Also, as transition onset approached, the relative positions of the peak positive and negative fluctuation velocities changed considerably; the peak negative values moved towards the boundary-layer edge and the peak positive ones moved towards the wall. This is the first time such measurements have been recorded and clearly illustrate the crucial information gained over r.m.s. distributions.

An experimental measure of the penetration depth of disturbances into the boundary layer has been defined using the skewness function. It was observed that the location of peak skewness, which had a negative value for the majority of the experiments, penetrated further into the boundary layer as the free-stream turbulence intensity and length scale increased. It was found that the variation of this penetration depth of disturbances (PD) was best represented by the following relationship, $PD \propto (\omega Re_x \tau_w)^{-0.3}$ which compares well to recent theoretical results based on solutions to the Orr–Sommerfeld equation about a piecewise linear velocity profile by Jacobs & Durbin (1998). The previous relationship can be simplified to rely only on free-stream parameters, thus avoiding any problems with accurate prediction of τ_w, as $PD \propto (\omega \rho U_e^2 \sqrt{Re_x})^{-0.31}$, therefore allowing for easy implementation into commercial codes. These results demonstrate the usefulness of the skewness parameter in giving an indication of the change in receptivity of a laminar boundary layer when under the influence of elevated free-stream turbulence intensity.

From the experimental results presented in this investigation, and in conjunction with DNS results, a more complete description of the bypass transition process is possible. The upward displacement of fluid in the free stream, owing to the movement of vortical structures in that region, causes the linear lift-up of the low-speed streaks from the wall towards the boundary-layer edge and further out into the free stream. The fluctuations measured on the lifted low-speed streaks near the boundary-layer

edge can have peak disturbance magnitudes of over 40 % of the free-stream velocity, approximately 5–10 % (relative to U_∞) greater than the disturbances associated with the peak positive fluctuations, thus illustrating the propensity of the boundary layer to induce transition on the deflected low-speed regions of the flow. The high-frequency disturbances from the free stream act on the low-speed streaks (backward jets) that are lifted towards the boundary-layer edge and the ensuing instabilities grow and intensify to the point where the flow eventually breaks down into turbulent motion. This turbulent motion then propagates towards the wall where near-wall turbulent structures with positive fluctuation velocity are observed at a downstream location.

This paper has emanated from research conducted with the financial support of Science Foundation Ireland (SFI). D. H. wishes to thank the H. T. Hallowell Jr Graduate Scholarship for financial assistance during the course of this investigation and also thank Dr Marc Hodes and Dr Alan Lyons of BLI for allowing him the time to complete his studies.

REFERENCES

Abu-Ghannam, B. J. & Shaw, R. 1980 Natural transition of boundary layers: the effects of turbulence, pressure gradient, and flow history. *IMechE* **22**, 213–228.

Andersson, P., Breggren, M. & Henningson, D. S. 1999 Optimal disturbances and bypass transition in boundary layers. *Phys. Fluids* **11**, 134–150.

Blair, M. F. 1992 Boundary-layer transition in accelerating flows with intense freestream turbulence: Part 1. Disturbances upstream of transition onset. *J. Turbomach.* **114**, 313–321.

Brandt, L., Schlatter, P. & Henningson, D. S. 2004 Transition in boundary layers subject to free-stream turbulence. *J. Fluid Mech.* **517**, 167–198.

Chong, T. P. & Zhong, S. 2005 On the three-dimensional structure of turbulent spots. *J. Turbomach.* **127**, 545–551.

Dryden, H. L. 1937 Airflow in the boundary layer near a plate. *NACA Rep. 562.*

Fransson, J. H. M. 2004 Leading edge design process using a commercial flow solver. *Exps. Fluids* **37**, 929–932.

Fransson, J. H. M., Matsubara, M. & Alfredsson, P. H. 2005 Transition induced by free-stream turbulence. *J. Fluid Mech.* **527**, 1–25.

Hammerton, P. W. & Kerschen, E. J. 1996 Boundary-layer receptivity for a parabolic leading edge. *J. Fluid Mech.* **310**, 243–267.

Hernon, D. & Walsh, E. J. 2007 Enhanced energy dissipation rates in laminar boundary layers subjected to elevated levels of freestream turbulence. *Fluid Dyn. Res.* **39**, 305–319.

Hernon, D., Walsh, E. J. & McEligot, D. M. 2006 An investigation using wavelet analysis into velocity perturbations under the influence of elevated freestream turbulence at transition onset. *ASME Paper* GT2006-90987.

Hinze, J. O. 1975 *Turbulence*. McGraw-Hill.

Hunt, J. C. R. & Durbin, P. A. 1999 Perturbed vortical layers and shear sheltering. *Fluid Dyn. Res.* **24**, 375–404.

Jacobs, R. G. & Durbin, P. A. 1998 Shear sheltering and the continuous spectrum of the Orr–Sommerfeld equation. *Phys. Fluids* **10**, 2006–2011.

Jacobs, R. G. & Durbin, P. A. 2001 Simulations of bypass transition. *J. Fluid Mech.* **428**, 185–212.

Johnson, M. W. 2001 On the flow structure within a turbulent spot. *Intl J. Heat Fluid Flow* **22**, 409–416.

Jonas, P. & Mazur, O. & Uruba, V. 2000 On the receptivity of the by-pass transition to the length scale of the outer stream turbulence. *Eur. J. Mech.* B/*Fluids* **19**, 707–722.

Kavence, G. & Oka, S. 1973 Correcting hot-wire readings for influence of fluid temperature variations. *DISA Information.* **15**, 21–24.

Kendall, J. M. 1985 Experimental study of disturbances produced in a pre-transitional laminar boundary layer by weak free-stream turbulence. *AIAA Paper* 85-1695.

KENDALL, J. M. 1998 Experiments on boundary-layer receptivity to freestream turbulence. *AIAA Paper* 98-0530.

KLEBANOFF, P. S. 1971 Effect of freestream turbulence on the laminar boundary layer. *Bull. Am. Phys. Soc.* **10**, 1323.

KUAN, C. L. & WANG, T. 1990 Investigation of intermittent behavior of transitional boundary layer using conditional averaging technique. *Expl Thermal Fluid Sci.* **3**, 157–170.

LANDAHL, M. T. 1975 Wave breakdown and turbulence. *SIAM J. Appl. Maths* **28**, 735–756.

LANDAHL, M. T. 1980 A note on an algebraic instability of inviscid parallel shear flows. *J. Fluid Mech.* **98**, 243–251.

LUCHINI, P. 2000 Reynolds-number-independent instability of the boundary layer over a flat surface: Optimal perturbations. *J. Fluid Mech.* **404**, 289–309.

MASLOWE, S. A. & SPITERI, R. J. 2001 The continuous spectrum for a boundary layer in a streamwise pressure gradient. *Phys. Fluids* **13**, 1294–1299.

MATSUBARA, M. & ALFREDSSON, P. H. 2001 Disturbance growth in boundary layers subjected to free-stream turbulence. *J. Fluid Mech.* **430**, 149–168.

MAYLE, R. E. 1991 The role of laminar–turbulent transition in gas turbine engines. *J. Turbomach.* **113**, 509–537.

ROACH, P. E. 1987 The generation of nearly isotropic turbulence by means of grids. *J. Heat Fluid Flow* **8**, 82–92.

ROACH, P. E. & BRIERLEY, D. H. 2000 Bypass transition modelling: a new method which accounts for free-stream turbulence intensity and length scale. *ASME Paper* 2000-GT-0278.

SARIC, W. S., REED, H. L. & KERSCHEN, E. J. 2002 Boundary-layer receptivity to freestream disturbances. *Annu. Rev. Fluid Mech.* **34**, 291–319.

SCHLICHTING, H. 1979 Boundary Layer Theory, 7th edn. McGraw-Hill.

UBALDI, M., ZUNINO, P., CAMPORA, U. & GHIGLIONE, A. 1996 Detailed velocity and turbulence measurements of the profile boundary layer in a large scale turbine cascade. *ASME Paper* 96-GT-4.

WALSH, E. J., HERNON, D., DAVIES, M. R. D. & MCELIGOT, D. M. 2005 Preliminary measurements from a new flat plate facility for aerodynamic research. *Proc. 6th European Turbomachinery Conference, March, Lille, France.*

WESTIN, K. J. A., BAKCHINOV, A. A., KOZLOV, V. V. & ALFREDSSON, P. H. 1998 Experiments on localized disturbances in a flat plate boundary layer. Part 1. The receptivity and evolution of a localized free stream disturbance. *Eur J. Mech.* B/*Fluids.* **17**, 823–846.

WU, X., JACOBS, R. G., HUNT, J. C. R. & DURBIN, P. A. 1999 Simulation of boundary layer transition induced by periodically passing wakes. *J. Fluid Mech.* **398**, 109–153.

WUNDROW, D. W. & GOLDSTEIN, M. E. 2001 Effect on a laminar boundary layer of small-amplitude streamwise vorticity in the upstream flow. *J. Fluid Mech.* **426**, 229–262.

WYGNANSKI, I., SOKOLOV, M. & FRIEDMAN, D. 1976 On a turbulent 'spot' in a laminar boundary layer. *J. Fluid Mech.* **78**, 785–819.

ZAKI, T. A. & DURBIN, P. A. 2005 Mode interaction and the bypass route to transition. *J. Fluid Mech.* **531**, 85–111.